physica status solidi rrl
www.pss-rapid.com

Stark-Localization-Limited Franz–Keldysh Effect in InAlAs Digital Alloys

*Yuan Yuan, Jiyuan Zheng, Keye Sun, Andrew H. Jones, Ann K. Rockwell, Stephen D. March, Yang Shen, Seth R. Bank, and Joe C. Campbell**

The optical absorption characteristics of the InAlAs digital alloy semiconductor are investigated. The external quantum efficiency of the InAlAs digital alloy is compared with that of the $In_{0.52}Al_{0.48}As$ random alloy. Unlike the random alloy, the digital alloy exhibits electric-field-induced Stark localization, which increases the optical absorption and suppresses the Franz–Keldysh red shift of the optical absorption edge.

The influence of an electric field on the optical absorption edge in semiconductors has been studied both theoretically and experimentally.[1–3] For random alloys, which are classified as bulk semiconductors, the conduction and valence band widths $\Delta E_{c,v}$ are of the order of a few eV.[4] An applied electric field gives rise to the Franz–Keldysh effect; the optical absorption coefficient exhibits an exponential tail below the bandgap.[4–6] Typically, for multi-quantum-well (MQW) semiconductors, the wells are relatively independent and the energy levels are discrete, i.e., $\Delta E_{c,v} \sim 0$. An applied electric field leads to the quantum-confined Stark effect (QCSE), which is observable as a red shift in the optical absorption edge.[3]

Recently, a semiconductor growth technology has advanced to enable the growth of high-quality, very short-period (e.g., tens of Å) semiconductor structures. These are referred to as digital alloys, which can be thought of as ultrathin superlattices.[7–13] The extremely thin periods, only a few monolayers (MLs), allow wave functions to couple through several wells by the resonant tunneling effect.[14] This results in a structure in which there is a quasicontinuum of energy levels, i.e., minibands with finite ΔE_c, as shown in **Figure 1**a. The widths of the conduction and valence minibands are typically tens of meV, an order of magnitude less than the energy band width of random alloys. Therefore, a moderate electric field, F, along the digital alloy growth direction can achieve $eFd \sim \Delta E_{c,v}$, where d is the digital alloys period thickness. In this circumstance, the relative energy misalignment reduces the tunneling effect and splits the quasicontinuum of states into discrete energy levels,[15] as shown in Figure 1b. In a random alloy, it is difficult to achieve the same before avalanche breakdown because $\Delta E_{c,v} \sim$ few eV and the lattice constant is a few Å ($F = \frac{\Delta E_{c,v}}{ed} \sim 10^7$ V cm^{-1}).

The threshold energy for optical absorption is determined by the energy difference from the top of the valence band state to the bottom of the conduction band state. For digital alloys, the electric-field-induced Stark localization of carriers to isolated quantum wells causes the energy difference to be reduced by $\frac{1}{2}\Delta E_c + \Delta E_v$. The optical absorption edge of a digital alloy semiconductor is expected to exhibit a suppressed Franz–Keldysh red shift as a result of this Stark localization effect when compared with the random alloys.[16]

In this letter, the electric-field-induced Stark localization of 8ML InAlAs digital alloys is reported. The digital alloy period consists of four MLs InAs and four MLs AlAs; the total thickness of a period is eight MLs (≈23 Å). The period structure of the 8ML InAlAs digital alloy observed by transmission electron microscopy (TEM) is shown in **Figure 2**. The study by Rockwell et al.[9] describes the material structure in more detail.

The absorption coefficients of the digital alloy and the random alloy have been determined by measuring the external quantum efficiency (EQE) of p-i-n photodiodes under different bias voltages. Both types of photodiodes have 600 nm depletion width; a schematic cross section is shown in **Figure 3**.[13] The three (p-type, unintentionally doped (UID), and n-type) InAlAs layers are all either digital alloys or random alloys. By the band structure simulation, the built-in voltage of the p-i-n photodiodes is ≈1.2 V, which results in ≈20 kV cm^{-1} built-in electric field in the UID InAlAs region. **Figure 4** shows the C–V curves of the digital and random alloy devices with an applied reverse voltage from 0 to −12 V (20–220 kV cm^{-1}), indicating both intrinsic layers have low background doping, and both depletion widths are weakly changed with electric field.

To distinguish the Stark localization in the digital alloy from the Franz–Keldysh effect in the $In_{0.52}Al_{0.48}As$ (InAlAs in the following) random alloy, their absorption characteristics are compared as functions of the electric field. The EQE was measured with 1 nm resolution using a SPEX 1681 spectrometer, a tungsten-halogen light source, and a lock-in amplifier, by comparing the device responsivities to those of a calibrated photodetector.

Y. Yuan, Dr. J. Zheng, Dr. K. Sun, A. H. Jones, Dr. Y. Shen, Prof. J. C. Campbell
Electrical and Computer Engineering Department
University of Virginia
351 McCormick Road, Charlottesville, VA 22904, USA
E-mail: jcc7s@virginia.edu

A. K. Rockwell, S. D. March, Prof. S. R. Bank
Electrical and Computer Engineering Department
University of Texas at Austin
1616 Guadalupe, St. Austin, TX 78758, USA

The ORCID identification number(s) for the author(s) of this article can be found under https://doi.org/10.1002/pssr.201900272.

DOI: 10.1002/pssr.201900272

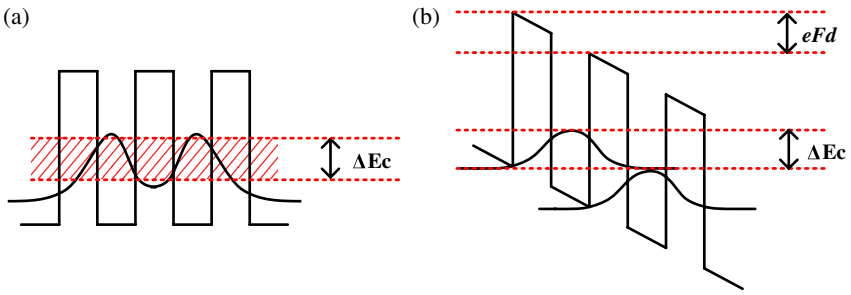

Figure 1. The overlap of wave functions throughout the digital alloys with a) small and b) $F \sim \Delta E_c/ed$ electric field.

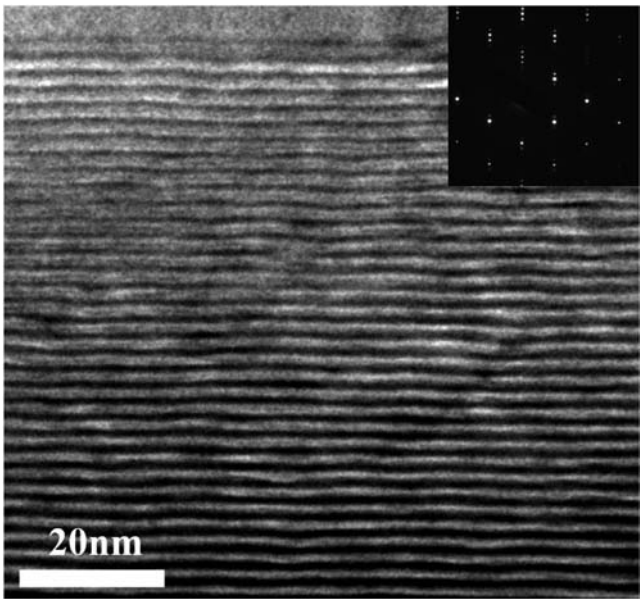

Figure 2. TEM picture under $g = (002)$ for the 8ML InAlAs digital alloy.

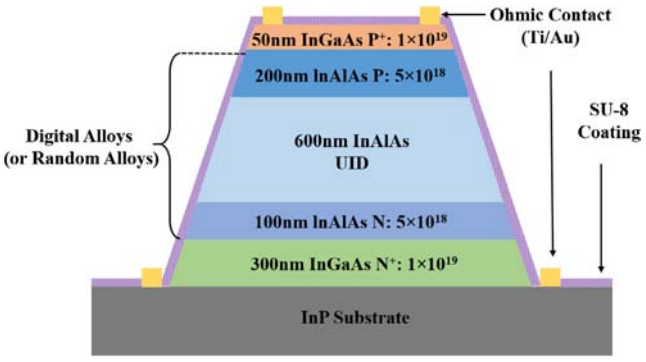

Figure 3. Schematic cross section of InAlAs digital alloy and random alloy photodiodes.

The measured quantum efficiencies of the digital and random alloys for reverse voltages from 0 to −12 V (20–220 kV cm^{-1}) are shown in **Figure 5**a,b, respectively. Similar to a GaAs-$Ga_{0.7}Al_{0.3}As$ superlattice with a well width of 50 Å and a barrier

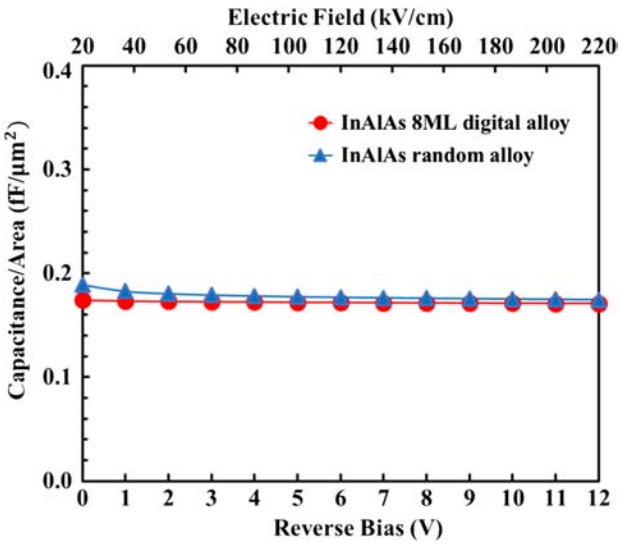

Figure 4. Capacitance–voltage (electric field) relationship for the digital and random InAlAs alloys.

width of 50 Å, which is shown in Figure 5c,[16] the quantum efficiency of the InAlAs digital alloy increases from 20 to 87 kV cm^{-1} and saturates at higher fields. Comparatively, the quantum efficiency of the InAlAs random alloy for photon energy higher than the bandgap is almost independent of the bias voltage.

The increased quantum efficiency of InAlAs digital alloy from 20 to 87 kV cm^{-1} is not caused by background doping because both digital alloy and random alloy photodiodes already completely depleted at very low electric field. In other words, this electric-field-dependent quantum efficiency for the digital alloy is due to the similar effect in the superlattice, which is shown in **Figure 6**. For simplicity, we assume there is only one miniband in each digital alloy potential.[17] At zero electric field, the wave functions extend throughout the digital alloys, as shown in Figure 6a, and the interband transitions are delocalized. At an intermediate electric field, in this case 20–87 kV cm^{-1}, the digital alloy energy states in the valence band still exhibit some delocalization. The eigenfunction of each quantum well is a Bessel function,[4] as shown in Figure 6b. Additional increase in the electric field will restrict the eigenfunction further in the quantum well, and after Fourier transform, there are more valance band energy states in the q space, where q is the wave vector in the digital alloy growth direction,[16] which leads to a higher quantum efficiency.

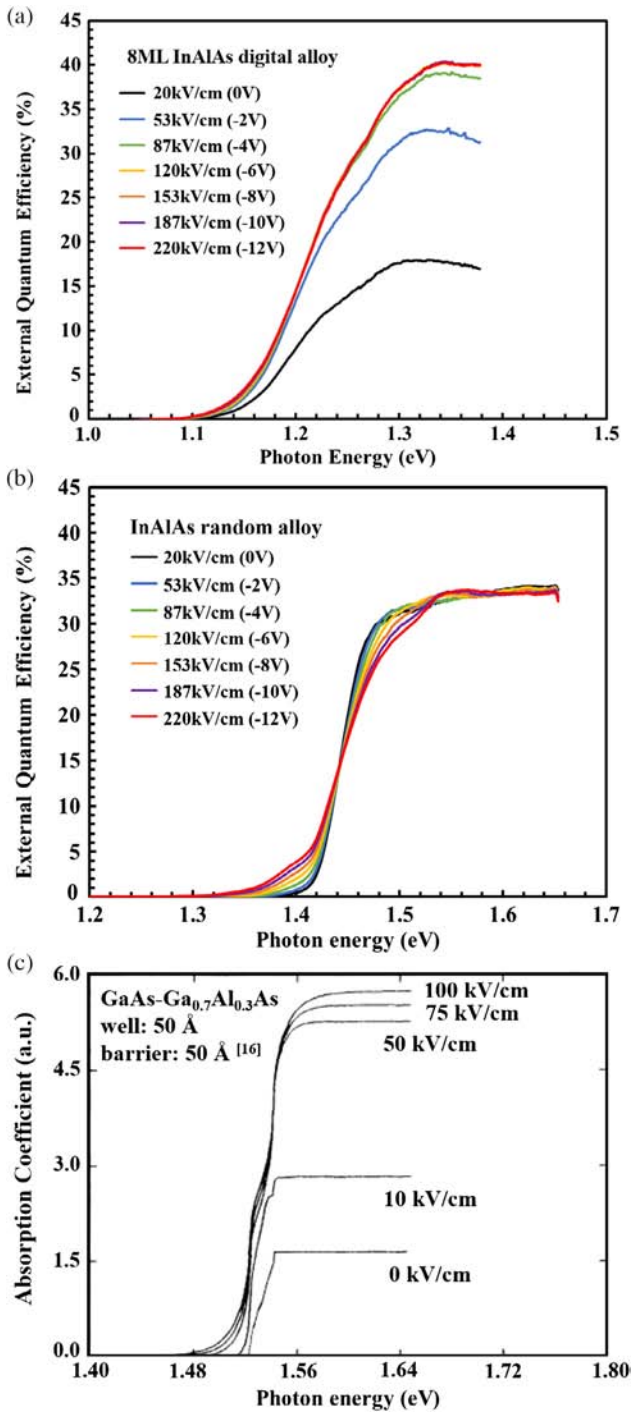

Figure 5. The EQE of a) 8ML InAlAs with digital alloy with a well width of 12 Å and a barrier width of 12 Å and b) InAlAs random alloy. c) The absorption coefficient of a GaAs–$Ga_{0.7}Al_{0.3}As$ superlattice with a well width of 50 Å and a barrier width of 50 Å.[16]

At high electric field, $F > \Delta E_{v,1}/ed$, the tunneling effect in the valence band is quenched. The valence band eigenfunctions are completely localized in the InAs quantum wells, as shown in Figure 6c, and the energy states in the q space no longer increase. Therefore, the quantum efficiency saturates.

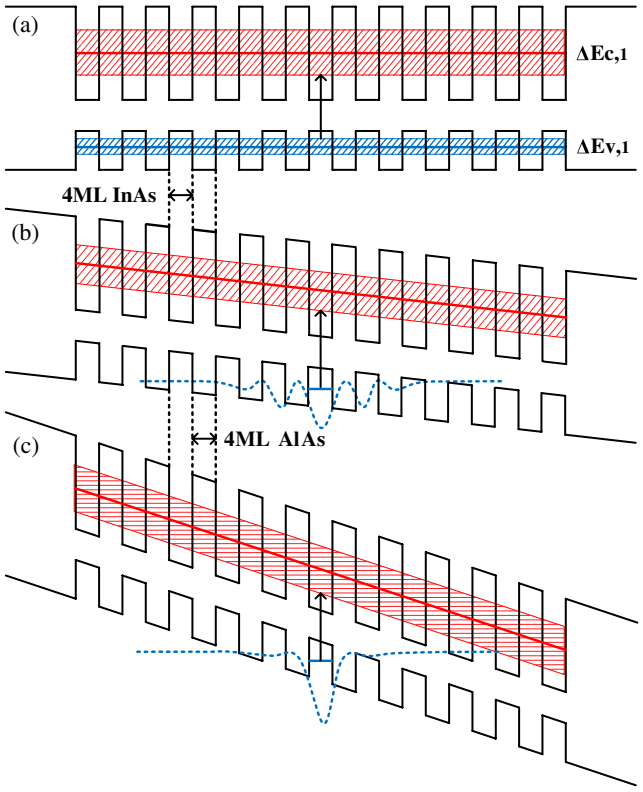

Figure 6. The conduction band and valence band potential profiles for InAlAs digital alloys under a) small, b) moderate, and c) high electric field.

The density of states for the InAlAs digital alloy has been calculated using an environment-dependent tight binding model.[18] **Figure 7** shows the bandgap $E_g \sim 1.13$ eV, the first miniband in the conduction band $\Delta E_{c,1} \sim 400$ meV, and the first miniband in the valence band $\Delta E_{v,1} \sim 46$ meV. The order of magnitude difference between ΔE_c and ΔE_v is caused by the higher effective mass in the valence band, $m_v^* \sim 0.75\, m_0 > m_c^* \sim 0.09\, m_0$. Therefore, for the InAlAs digital alloy, only the energy states in the valence band exhibit Stark localization. Based on this calculation, the effective blue shift from the Stark localization is expected to be $\approx \frac{1}{2}\Delta E_{v,1}$.

To verify the suppressed red shift prediction for the InAlAs digital alloy, the measured EQEs are also plotted with log-scale in **Figure 8**. Note that the quantum efficiency minimum is limited to 0.1% by the magnitude of the photoresponse at this level, and the lock-in amplifier accuracy caused some oscillation in the low quantum efficiency region. The absorption edge of the InAlAs digital alloy changes ≈15 nm (≈14 meV) from 20 to 220 kV cm^{-1}, whereas that of the InAlAs random alloy is ≈52 nm (≈76 meV). The observed cutoff wavelength difference between the digital and random alloys is expected, as per the study by Rockwell et al.[9] The red shift in the random alloy is due to the well-known Franz–Keldysh effect. The energy band profile tilts along the direction of the electric field, and a photon with energy slightly below the bandgap can be absorbed by the photon-assisted interband tunneling. The absorption coefficient exhibits an exponential tail below the bandgap

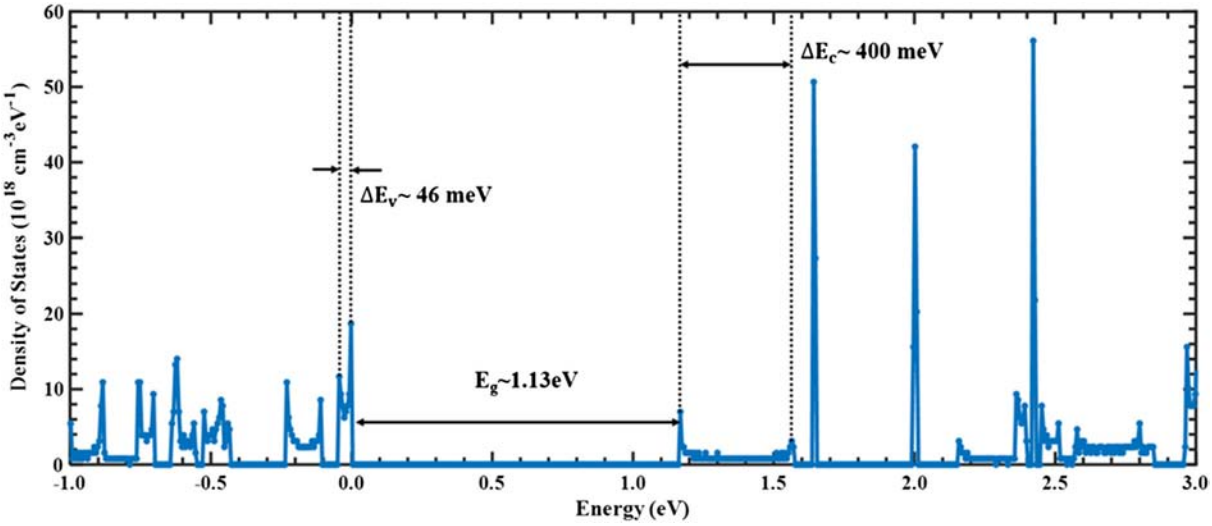

Figure 7. The density of states for 8ML InAlAs digital alloy.

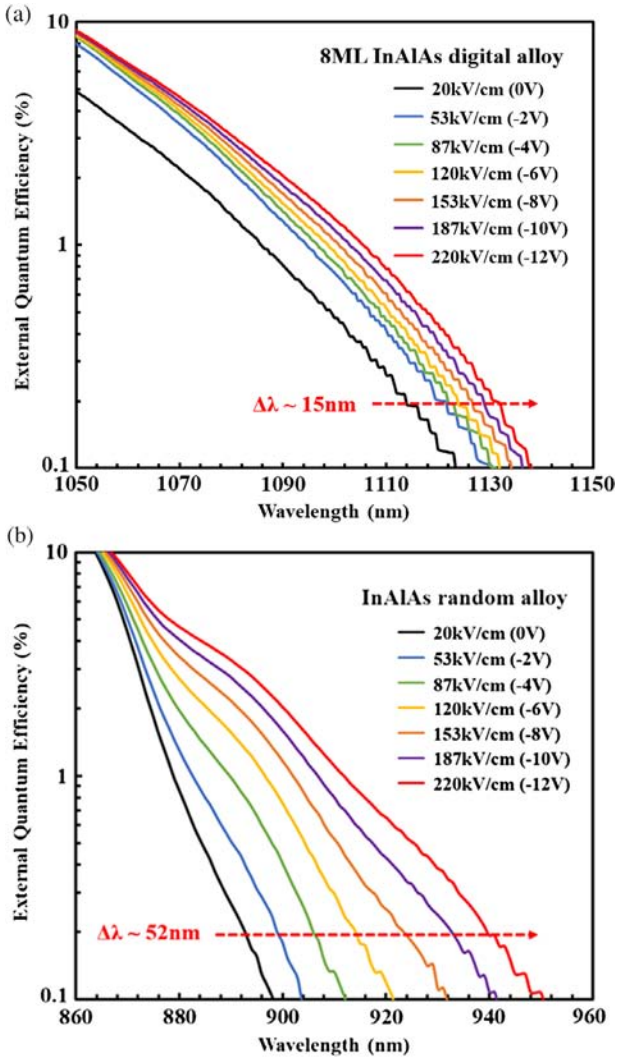

Figure 8. The absorption edge of a) 8ML InAlAs digital alloy and b) InAlAs random alloy.

$$\alpha(\hbar\omega) \propto \sqrt{\hbar\theta_F}[-\eta \mathrm{Ai}^2(\eta) + \mathrm{Ai}'^2\eta] \quad (1)$$

where $\hbar\theta_F = (\hbar^2 e^2 F^2 / 2m_r^*)^{1/3}$, m_r^* is the reduced mass, $\eta = (E_g - \hbar\omega)/\hbar\theta_F$, $\mathrm{Ai}(\eta)$ is the Airy function, and $\mathrm{Ai}'(\eta)$ is the derivative of $\mathrm{Ai}(\eta)$ with respect to η.[19] The Franz–Keldysh effect in the random alloy has ≈76 meV red shift from 20 to 220 kV cm^{-1}. However, since m_r^* of the InAlAs digital alloy (≈0.08 m_0) is larger than that of the InAlAs random alloy (≈0.06 m_0), the red shift of the digital alloy caused by the Franz–Keldysh effect should be smaller, ≈40 meV. The measured red shift of the digital alloy is only ≈14 meV. Although, the cutoff wavelength still extends to longer wavelengths with increasing field, the change in absorption edge is effectively suppressed. At zero electric field, the InAlAs digital alloy bandgap energy corresponds to the difference between the bottom of the conduction miniband and the top of the valence miniband, ≈1.13 eV, and at high bias voltage, this energy gap is reduced to half of the valence miniband ≈23 meV by the Stark localization effect. It leads to the suppressed red shift, which is consistent with the measured value.

In conclusion, by measuring the EQEs of an InAlAs digital alloy and an InAlAs random alloy under different applied electric fields, the absorption characteristics of these two semiconductors were investigated. Due to the Franz–Keldysh effect, both absorption edges exhibit a red shift. However, electric-field-induced Stark localization of the digital alloy results in an electric-field-dependent quantum efficiency and an effectively suppressed red shift.

Acknowledgements

The authors would like to thank Dr. Yukun Sun and Dr. Minjoo Larry Lee at the Department of Electrical and Computer Engineering, University of Illinois at Urbana-Champaign, for helping them take the TEM image. This work was supported by the Army Research Office (W911NF-17-1-0065) and DARPA (GG11972.153060).

Conflict of Interest

The authors declare no conflict of interest.

Keywords

digital alloys, Franz–Keldysh effect, Stark localization

Received: May 12, 2019
Revised: May 26, 2019
Published online:

[1] D. A. B. Miller, D. S. Chemla, T. C. Damen, A. C. Gossard, W. Wiegmann, T. H. Wood, C. A. Burrus, *Phys. Rev. B* **1985**, *32*, 1043.
[2] D. A. B. Miller, D. S. Chemla, T. C. Damen, A. C. Gossard, W. Wiegmann, T. H. Wood, C. A. Burrus, *Phys. Rev. Lett.* **1984**, *53*, 2173.
[3] D. A. B. Miller, D. S. Chemla, S. Schmitt-Rink, *Phys. Rev. B* **1986**, *33*, 6976.
[4] J. Bleuse, G. Bastard, P. Voisin, *Phys. Rev. Lett.* **1988**, *60*, 220.
[5] W. Franz, *Z. Naturforsch.* **1958**, *13a*, 484.
[6] L. V. Keldysh, *Sov. Phys.* **1958**, *7*, 788.
[7] S. J. Maddox, S. D. March, S. R. Bank, *Cryst. Growth Des.* **2016**, *16*, 3582.
[8] M. Ren, S. J. Maddox, M. E. Woodson, Y. Chen, S. R. Bank, J. C. Campbell, *J. Lightwave Technol.* **2017**, *35*, 2380.
[9] A. K. Rockwell, M. Ren, M. Woodson, A. H. Jones, S. D. March, Y. Tan, Y. Yuan, Y. Sun, R. Hool, S. J. Maddox, M. L. Lee, A. W. Ghosh, J. C. Campbell, S. R. Bank, *Appl. Phys. Lett.* **2018**, *113*, 102106.
[10] S. R. Bank, J. C. Campbell, S. J. Maddox, A. K. Rockwell, M. E. Woodson, M. Ren, A. H. Jones, S. D. March, J. Zheng, Y. Yuan, in *IEEE Research and Applications of Photonics In Defense (RAPID) Conference*, Miramar Beach, FL, Aug. **2018**, IEEE **2018**, pp. 1–3.
[11] Y. Yuan, A. K. Rockwell, Y. Peng, J. Zheng, S. D. March, A. H. Jones, M. Ren, S. R. Bank, J. C. Campbell, *J. Lightwave Technol.* **2019** (accepted).
[12] J. Zheng, Y. Yuan, Y. Tan, Y. Peng, A. K. Rockwell, S. R. Bank, A. W. Ghosh, J. C. Campbell, *J. Lightwave Technol.* **2018**, *36*, 3580.
[13] Y. Yuan, J. Zheng, Y. Tan, Y. Peng, A. K. Rockwell, S. R. Bank, A. W. Ghosh, J. C. Campbell, *Photon. Res.* **2018**, *6*, 794.
[14] J. Zheng, Y. Tan, Y. Yuan, A. W. Ghosh, J. C. Campbell, *J. Appl. Phys.* **2018**, *125*, 082514.
[15] E. E. Mendez, G. Bastard, *Phys. Today* **1993**, *46*, 34.
[16] B. Jogai, K. L. Wang, *Phys. Rev. B* **1987**, *35*, 653.
[17] E. E. Mendez, F. Agullo-Rueda, J. M. Hong, *Phys. Rev. Lett.* **1988**, *60*, 2426.
[18] Y. Tan, M. Povolotskyi, T. Kubis, T. B. Boykin, G. Klimeck, *Phys. Rev. B* **2016**, *94*, 045311.
[19] S. L. Chuang, *Physics of Photonic Devices*, Vol. *80* of Wiley Series in Pure and Applied Optics, John Wiley & Sons, New York **2012**.